Desalination and Water Treatment
www.deswater.com

doi: 10.5004/dwt.2019.23917

151 (2019) 403–413
May

Gum Arabic dialdehyde thiosemicarbazone chelating resin for removal mercury (II) from aqueous solutions

Adel A. El-Zahhar[a,b,*], Samir Bondock[a,c], Mohammad Abu Haija[d], Sherif M.A.S. Keshk[a,e]

[a]*Department of Chemistry, College of Science, King Khalid University, P.O. Box 9004, Abha 61413, Saudi Arabia, Tel. +966172418634; email: elzahhar@kku.edu.sa (A.A. El-Zahhar)*
[b]*Nuclear Chemistry Department, Hot Labs. Center, Atomic Energy Authority, P.C.13759, Cairo, Egypt*
[c]*Chemistry Department, Faculty of Science, Mansoura University, Mansoura 35516, Egypt*
[d]*Department of Chemistry, Khalifa University of Science and Technology, SAN Campus, PO Box 2533, Abu Dhabi, UAE*
[e]*Department of Basic Science, Institute of Environmental Studies and Research, Ain Shams University, Abbassia, Cairo, Egypt*

Received 22 September 2018; Accepted 3 February 2019

ABSTRACT

In continuation of our efforts to explore the application of a modified natural polymer to remove toxic heavy metals from aqueous solutions, Gum Arabic (Gum acacia [GA]) dialdehyde phenylthiosemicarbazone (GAD-PTSC) chelating resin was prepared through the oxidation of GA followed by a reaction with 4-phenylthiosemicarbazide (PTSC). The structural functionalities, surface morphologies, and thermal stabilities of the resultant adsorbent resin were characterized using Fourier-transform infrared spectroscopy (FTIR), scanning electron microscopy (SEM), and thermo-gravimetric analysis. The chelating behavior of the obtained resin with mercury (Hg (II)) in aqueous solution was studied using the batch technique. The adsorption and the kinetic models were adopted to calculate the kinetic and thermodynamic parameters of the adsorption process. The removal percentage of Hg (II) ions on GAD-PTSC reached 97% at pH 5.5, and the maximum adsorbed amount of Hg (II) was found to be 120 mg g^{-1} at pH 5.5. The experimental results complied with the second-order kinetic model supporting chemical adsorption with calculated maximum adsorption capacity of 122.10 mg g^{-1}. The Langmuir isotherm model showed good fitting with the experimental results with maximum adsorption capacity of 133.33 mg g^{-1}.

Keywords: Gum Arabic dialdehyde phenylthiosemicarbazone; Hg(II); Adsorption; Kinetics; Thermodynamics

1. Introduction

The presence of mercury (Hg) in water and environment is a serious threat to human health. Generally, mercury is introduced to water and environment as a by-product of different industries, such as batteries, alloys, and chemicals [1]. Mercury is known to highly toxic and affects the neurological and the renal system [2]. Different approaches were studied for decontamination and removal of pollutants. Phytoremediation process as an effective and eco-friendly procedure was studied and showed considerable efficiency for soil and water treatment [3]. Activated carbon derived from Spirogyra species was utilized for lead (II) removal from aqueous solutions and showed experimental removal efficiency of 96.6% [4]. The parameters controlling the adsorption of lead (II) ions were studied and optimized. Siva Rajasekar studied the adsorption of copper (II) ions in aqueous solutions using bio-sorbent material based on the activated carbon derived from rubber tree sawdust [5]. The adsorbent dose, solution pH, metal ion concentration and other affecting variables were studied.

The decontamination of mercury from water and wastewater has attracted significant attention. Several separation techniques, such as precipitation, reverse osmosis,

* Corresponding author.

ion exchange, electrodialysis, membrane filtration, and adsorption with chelating resins, have been proposed for the removal of heavy metal ions from aqueous solutions. Chelating resins are considered as one of the most used materials as adsorbents due to their ease of application and high selectivity and recyclability [6–8]. Different chelating resins have been prepared for the separation of heavy metal ions from aqueous solutions [9–14]. The chelating of mercury is considered of high importance [15–21]. Where, the selective decontamination and preconcentration of heavy metals including mercury have been studied using different chelating resins, such as amidoxime, magnetic chelating resins, polymeric resins, and composite resins [22–29]. Sulfur- and nitrogen-based chelating resins have been potentially used as donor atoms for the selective chelation with transition metals [30]. The chelating resins have been used in the separation of heavy metal ions from aqueous solutions with higher selectivity in the presence of alkali and alkaline earth metal ions [31]. Gum acacia (GA) is a heterogeneous polysaccharide and can be obtained from *Acacia senegal* var. *senegal trees*. GA consists of β-(1–3) linked galactose residues with branches linked at 1, 6 positions, and arabinose, rhamnose, and glucuronic acids which are in the ramified side chains [32]. The wide use of GA for the decontamination of water is due to its high solubility, good emulsifying characteristics, and low viscosity as compared with other polysaccharides [33]. Moreover, thiosemicarbazones and their metal complexes are also potential candidates for the removal of heavy metal ions from aqueous solutions due to their excellent biological activities, analytical uses, and remarkable chemical and structural properties [34]. The outstanding chemical and structural characteristics of thiosemicarbazide are due to the condensation of different carbonyls as well as through the alkylation of various parts of thiosemicarbazide moiety. Furthermore, the biological activity of thio-semicarbazones depends on the chemical nature of the moiety attached to the CS carbon atom [35]. In this study, we have synthesized and developed novel Schiff's base through condensation reaction of dialdehyde GA with phenylthiosemicarbazide to produce the novel chelating compound Gum Arabic dialdehyde-phenylthiosemicarbazide (GAD-PTSC). The obtained chelating Schiff's base GAD-PTSC was characterized using FTIR, SEM-EDX and thermo-gravimetric analysis (TGA) to determine the structural characteristics, surface morphology, elemental content and thermal stability. The prepared Schiff's base GAD-PTSC was studied for removal of Hg(II) from aqueous solutions for the first time. Different parameters affecting the uptake of Hg(II) were studied as: contact time, pH, temperature, and metal ion concentration. Furthermore, the adsorption kinetics, isotherms, thermodynamics and mechanism were studied.

2. Materials and methods

2.1. Materials

Gum Arabic (GA) powder, potassium periodate, and $HgCl_2$ were purchased from Sigma Aldrich. All chemicals were used as received without further purification.

2.2. Preparation of Gum Arabic 2, 3-dialdehyde (2, GAD)

In a solution of GA (1 g, 0.0055 mole) and 200 mL warm distilled water (DI), KIO_4 (1.5 g, 0065 mole) was added portion wise with stirring for 15 min, and the resultant solution was kept in dark and stirred for 24 h (Fig. 1). The reaction was quenched by 5 mL ethylene glycol to remove unreacted KIO_4. The solution was then centrifuged at 6,000 rpm for 15 min,

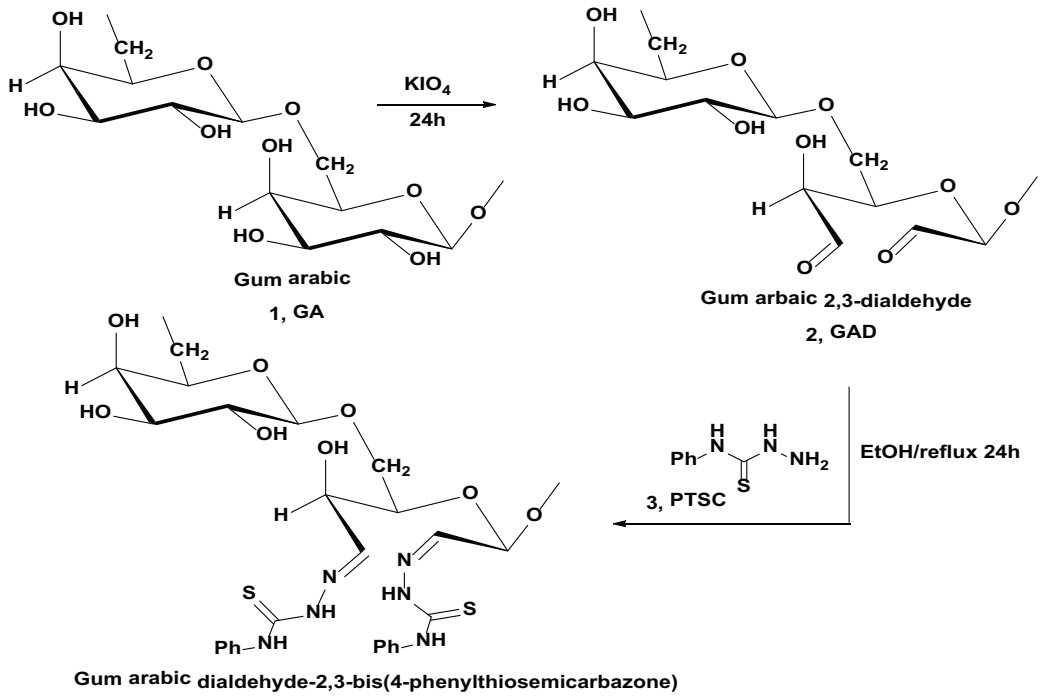

Fig. 1. Synthetic rout for the synthesis of Gum acacia dialdehyde-2,3-bis (4-phenyl thiosemicarbazone).

and the collected supernatant solution was treated with acetone in a 1:4 ratios to precipitate Gum Arabic 2,3-dialdehyde (2, GAD). The obtained GAD was dissolved in 250 mL DI and again re-precipitated by the addition of acetone. This process was repeated five times, and the final resultant GAD precipitate was freeze-dried and powdered.

2.3. Preparation of Schiff's base

Gum Arabic dialdehyde-2, 3-bis (4-phenylthiosemicarbazone) (4, GAD-PTSC) was prepared through the following procedure: in a solution of GAD (0.35 g, 0.002 mole), 4-phenylthiosemicarbazide (PTSC, 0.668g, 0.004 mole), 30 mL ethanol, and 0.1 mL concentrated hydrochloric acid (HCL) was added (Fig. 1).

The mixture was then heated under reflux for 4 h and cooled down to room temperature. The obtained pale-yellow powder of GAD-PTSC was collected by filtration, washed well three times with diluted ethanol, and dried under vacuum.

2.4. Characterization of the Schiff's base

Fourier-transform infrared spectrometer (FTIR; NICOLET 6700 Thermo Scientific) was employed to record the infrared spectra of GAD and GAD-PTSC using the pressed KBr discs. In order to observe morphologies of GAD and GAD-PTSC, scanning electron microscope (SEM-FEI; Quanta 200) was adopted. The samples were coated with gold prior to the SEM analysis. The thermal stability of the prepared resin was analyzed using the Shimadzu TGA-50H thermal analyzer. The sample (10 mg) was heated in a platinum crucible in the temperature range of 25°C– 600°C with a heating rate of 10°C/min under nitrogen atmosphere.

2.5 Metal ion adsorption using the batch method

Batch experiments were performed to study the removal of Hg (II) ions by GAD-PTSC. In 100 mL stoppered bottles, 0.05 g GAD-PTSC was added to 50 mL Hg (II) solution with a concentration of 100 mg L^{-1} at pH 6, and the resultant solution was kept at 25°C for 3 h. However, in order to study the adsorption isotherm, the initial concentration of metal ions was investigated in the range of 10–200 mg L^{-1}. In the thermodynamic study, the concentration of metal ions was 120 mg L^{-1}. Moreover, in order to study the influence of pH, the values of pH were in the range of 1–6; for the investigation of temperature effect, the temperature of the solution was extended between 25°C and 50°C; and for the study of kinetic behavior, the time of contact was changed from 5 to 120 min. All bottles were shaken by a thermostat shaker at 150 rpm. The resultant GAD-PTSC was taken, and the amount of residual metal ions in the solution was determined by the spectrophotometric method using (ethylenediaminetetraacetic acid) solution and (4-(2-pyridylazo)-resorcinol) indicator. The adsorption rate and the adsorbed amount of Hg (II) ions were calculated as below:

$$\text{Adsorption}\% = \left(\frac{C_0 - C_e}{C_0}\right) \times 100\% \quad (1)$$

$$q_e = \frac{V(C_0 - C_e)}{W} \quad (2)$$

where C_o and C_e are the initial and equilibrium Hg (II) concentrations, q_e is the equilibrium adsorption capacity (mg g^{-1}), W is the resin weight (g), and V is the solution volume (L). The Hg (II) uptake was considered as a function of pH and varied around 3–8 with an initial Hg (II) concentration of 10 mg L^{-1}. Adsorption equilibrium parameters were calculated as a function of temperatures (15°C, 25°C, 35°C, and 45°C). The initial Hg (II) concentration was between 0.1 and 250 mg L^{-1}. The effect of Hg (II) uptake was studied by shaking a predetermined amount of dry resin in aqueous solutions with different Hg (II) concentrations at pH 2. After reaching the equilibrium, the concentration of residual Hg (II) ions was determined. The Langmuir and Freundlich adsorption isotherm models were applied to the obtained experimental results, and the isotherm parameters were calculated.

2.6. Regeneration of the depleted resin

The regeneration of the Hg (II) loaded resin was performed by 0.5 M HCl solution as Hg(II) releasing solution. The saturated GAD-PTSC sample was mixed with 50 ml of HCl solution for 30 min. The regenerated samples were washed by distilled water many times and reused in repeated adsorption cycles, and the efficiency of the regenerated resin was determined.

3. Results and discussion

3.1. Characterization of the prepared resin

The FTIR spectra of GA, GAD, GAD-PTSC, and GAD-PTSC-Hg (II)) are displayed in Fig. 2. The peaks of GA at 3412, 2931 and 1608 cm^{-1} denote–OH stretching, $–CH_2$ stretching [36], and C-O asymmetric stretching vibrations, respectively. The absorption band at 1420 cm^{-1} denotes the wagging vibrations for CH and $–CH_2$ [37]. It can be ascribed to the skeletal motion of carbon rings. The absorption band of C–O–C linkage appeared at 1073 cm^{-1}, and the peak at 603 cm^{-1} can be attributed to C–H out-of-plane bending vibration. The changes in GA structure after the periodate oxidation were detected in the form of new absorption bands at 1728, 1046 and 757 cm^{-1} owing to C=O stretching, C–O–C stretching, and C–H out-of-plane bending vibrations, respectively. These bands also support the presence of hemiacetal and hydrated bonds between the aldehyde and the hydroxyl groups. It is worth noting that these characteristic peaks of GAD were also detected by Stefanovic et al. [38]. The FTIR spectrum of GAD-PTSC exhibited a new absorption band at 1616 cm^{-1} for the azomethine group (C=N). The strong peak at 1719 cm^{-1} represents the residual unreacted aldehyde group. The absorption bands at 1598, 1540, 1319, 1258, 753 and 694 cm^{-1} are the characteristic peaks for C=C stretching, C=S stretching, and C–H out-of-plane bending vibrations, respectively. The absorption bands of C=N and C=S (two coordination sites) appeared at 1600 and 1317 cm^{-1}, respectively. It is noticeable that these two peaks were slightly shifted to lower wave numbers with a decrease in the

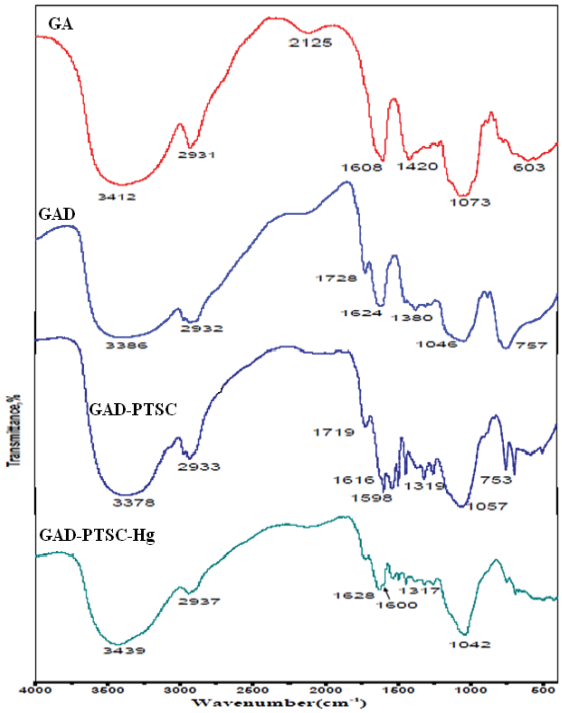

Fig. 2. FTIR spectra for GA, GAD, GAD-PTSC, and GAD-PTSC-Hg.

intensities; this feature confirms that GAD-PTSC behaves as an N, S- bidentate ligand.

The surface morphologies of GAD and GAD-PTSC samples were characterized by SEM, and the micrographs were recorded at different magnifications (Fig. 3). It was observed that the GAD-PTSC particles were smaller in size as compared with the GAD particles. It is evident at high magnifications that the surface of GAD-PTSC was more porous than GAD, which facilitates the access of Hg (II) ions to the inside of GAD-PTSC particles.

Fig. 4 compares the SEM images of GAD-PTSC before (Figs. 4(a) and (b) and after (Figs. 4(c) and (d) Hg (II) adsorption. After Hg (II) adsorption, the GAD-PTSC particles were arranged as flakes. Moreover, the surface of GAD-PTSC after adsorption was smoother as compared with the surface before adsorption; it can be attributed to the complexation between Hg (II) and GAD-PTSC.

The results of EDX analysis are presented in Table 1. The major elements for GAD were carbon (58.5 wt%) and oxygen (41.5 wt%), whereas GAD-PTSC contained carbon (63.4 wt%), oxygen (20.3 wt%), nitrogen (4.2 wt%), and sulfur (12.1 wt%). The EDX analysis for GAD-PTSC-Hg showed that the percentage of Hg in the sample reached 4.85% which confirms the adsorption of Hg on GAD-PTSC-Hg.

The TGA curves of GAD and GAD-PTSC samples manifest the mass losses in the temperature range of 25°C and 600°C (Fig. 5). The total weight loss for each sample was about 80%. The characteristics of the TGA curves for both samples signify a homogenous composition. The first thermal weight loss step involves the removal of absorbed water molecules was completed before 200°C. This step reflects the gradual dehydration of the sample [39]. The second step completed

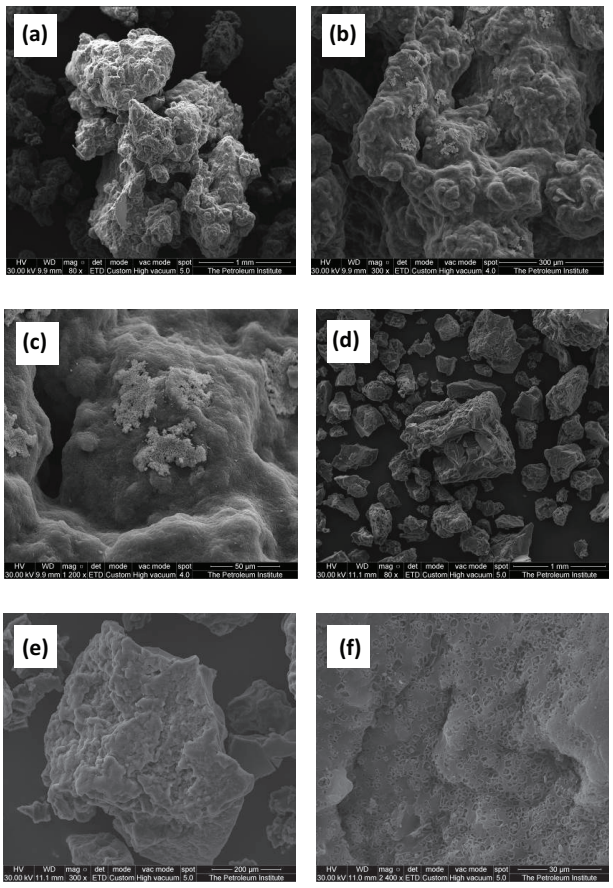

Fig. 3. SEM micrographs for GAD (a) – (c) and GAD-PTSC (d)–(f).

before 300°C involves the removal of crystalline water and then the decomposition of hydrocarbons. Unlike the GAD sample, the TGA curve of GAD-PTSC exhibited an extra weight loss step between 300°C and 500°C; this step involves the elimination of phenylthiosemicarbazone groups.

3.2. Metal ions uptake

3.2.1. Effect of pH on adsorption

The variation in pH of the solution has a significant effect on resin selectivity and adsorption capacity [40]. The adsorption of Hg (II) ions on GAD-PTSC at different pH values is displayed in Fig. 6. It can be seen that the maximum removal rate of Hg (II) ions from aqueous solutions was obtained at pH 4.5–5.5, which could be attributed to the complexation process between Hg (II) ions and the active groups of GAD-PTSC. However, the decrease in pH led to the protonation of functional groups, that hinders the reaction between Hg (II) ions and GAD-PTSC resin [41].

The removal percentage of Hg (II) ions on GAD-PTSC reached 97% at pH 5.5. The mechanism of Hg (II) adsorption could be explained by the formation of a complex between Hg (II) ions and the deprotonated functional groups, such as thiol-groups, of PTSC units. The release of H^+ ions was observed by noticing the decrease in final pH value. The FTIR spectra of GAD-PTSC before and after the adsorption of Hg^{2+} are displayed in Fig. 2. The presence of strong peaks at 1620

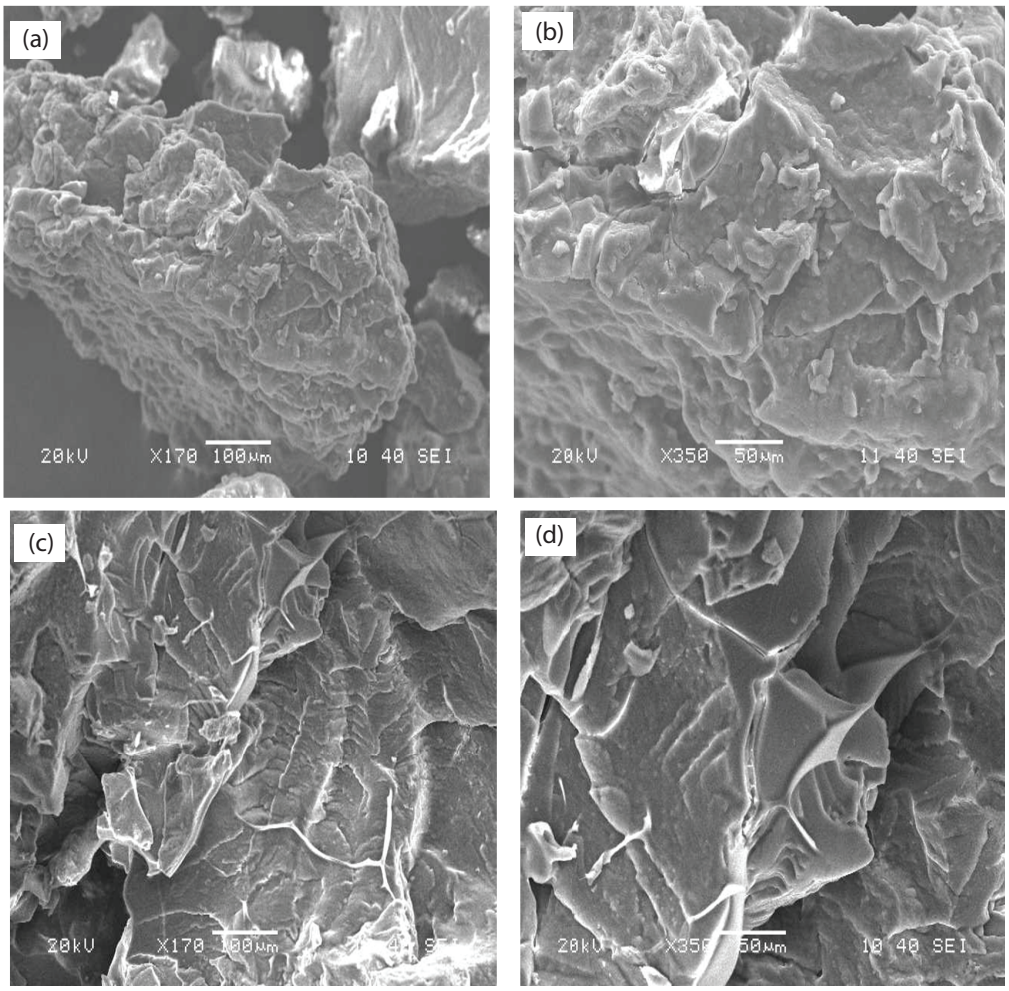

Fig. 4. SEM micrographs for GAD-PTSC (a) and (b), and GAD-PTSC-Hg (c) and (d).

Table 1
The EDX elemental analysis (weight%) of GAD, GAD-PTSC and GAD-PTSC-Hg

Samples	C	O	N	S	Hg
GAD	58.5	41.5	–	–	–
GAD-PTSC	63.4	20.3	4.2	12.1	–
GAD-PTSC-Hg	38.42	34.14	20.68	1.90	4.85

and 740 cm^{-1} indicates the C=N and C-S bonds, respectively. The disappearance of the peak at 1300 cm^{-1}, which corresponds to C=S, proves the adsorption of Hg (II) on GAD-PTSC resin [42].

The surface charge was studied as the ζ potential within the pH range of 2–9.5. The pH_{PZC} of the GAD-PTSC resin refers to pH value at which the charge density on the particle surface is zero; as the positive and negative charges are equivalent due to proton equilibrium. The isoelectric point for GAD-PTSC resin was found to be 5.5. This finding indicates that the resin surface was negatively charged at pH higher than 5.5 have and positive surface at lower pH than 6.5. This explain the increased adsorption of Hg (II) with increasing pH as the active groups of GAD-PTSC (hydroxyl group, carbonyl group and amino group) deprotonated with increasing the solution pH and turned negatively charged.

3.2.2. Effects of temperature and adsorption thermodynamics

The adsorption of Hg (II) on GAD-PTSC resin was investigated at different temperatures (25°C–50°C); and it was found that the adsorption decreased with the increasing reaction temperature (Fig. 7). Different thermodynamic parameter, such as Gibbs free energy change (Δ*G*°), enthalpy change (Δ*H*°), and entropy change (Δ*S*°), were calculated from the plot of $\ln K_c$ vs. $1/T$ (Fig. 7), and the obtained results are depicted in Table 2. The thermodynamic parameters were calculated by Eq. (3).

$$k_c = q_e/C_e \tag{3}$$

where q_e is the adsorbed amount of solute on the solid resin at equilibrium (mg g^{-1}) and C_e is the concentration of Hg (II) ions in solution at equilibrium (mg L^{-1}).

The free energy change for adsorption (Δ*G*°) of Hg (II) ions on GAD-PTSC was calculated using Eq. (4).

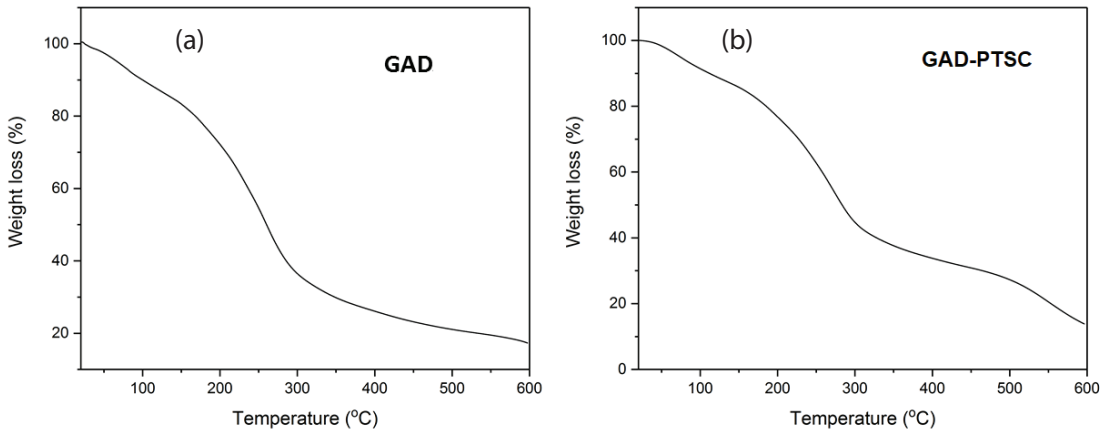

Fig. 5. TGA plots of GAD (a) and GAD-PTSC (b) samples heated at 10°C/min under nitrogen atmosphere.

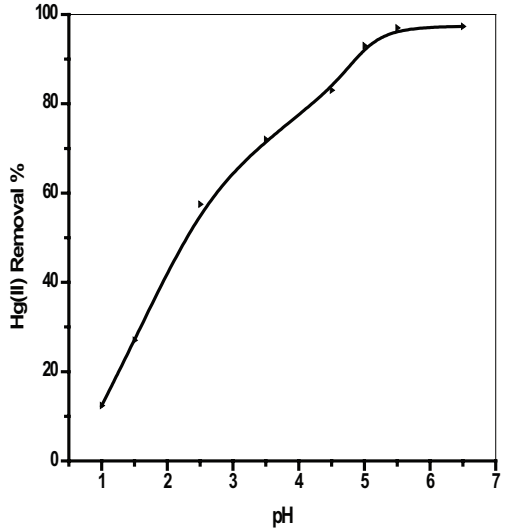

Fig. 6. Effect of pH on the removal of Hg (II) onto GAD-PTSC resin; Resin dose 0.1 g/50 mL, Temperature 23°C ± 0.1°C and contact time of 30 min.

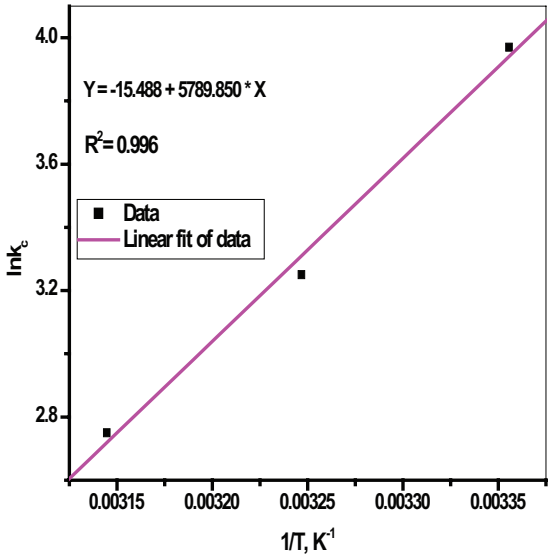

Fig. 7. Plot of lnK_c against (1/T) for the adsorption of Hg^{2+} onto GAD-PTSC resin.

$$\Delta G^\circ = RT\ln k_c \quad (4)$$

The standard enthalpy change (ΔH°) was calculated by Eq. (5).

$$\ln k_c = \frac{\Delta S^\circ}{R} - \frac{\Delta \mathrm{H}^\circ}{RT} \quad (5)$$

where R is the universal gas constant (8.314 J/mol K).

The calculated thermodynamic parameters are presented in Table 2. The negative value of ΔG° reflects a spontaneous and favorable reaction, whereas negative value of ΔH° implies that the adsorption reaction is exothermic in nature.

Table 2
Thermodynamic parameters for the adsorption of Hg^{2+} on GAA-TSC resin

Temperature (K)	k_c	ΔG° (kJ/mol)	ΔH° (kJ/mol)	ΔS° (J/mol)
298	52.98	–9.835	–48.136	–128.767
318	25.79	–8.592		
328	15.64	–7.498		

3.2.3. Effect of contact time

The adsorption of Hg (II) on GAD-PTSC resin was studied at different contact time periods to determine the time necessary for achieving the equilibrium. The results in Fig. 8 reveal that the adsorption rate initially increased with time, thus reflecting a fast adsorption reaction between functional groups of GAD-PTSC resin and Hg (II) ions. However, the adsorption rate became slow after 30 min. Therefore, the contact time necessary for reaching equilibrium between Hg (II) ions and GAD-PTSC was found to be 30 min.

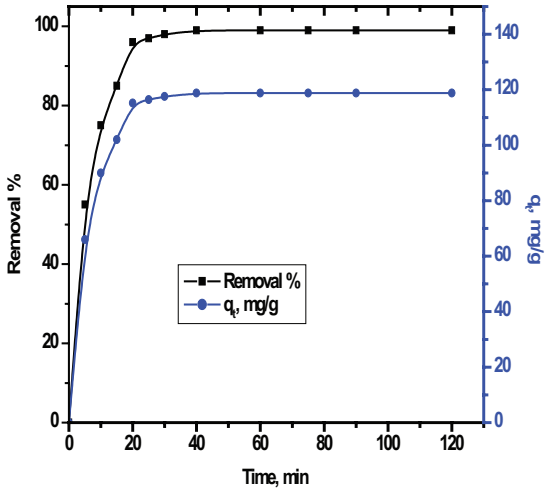

Fig. 8. Effect of contact time on the adsorption of Hg (II) onto GAD-PTSC; Adsorbent dose 0.1 g/100 mL, Temperature 25°C, [Hg (II)] is 120 mg L^{-1} and pH 6.

3.2.3.1. Adsorption kinetics Different kinetic models were applied to the obtained results to describe the adsorption mechanism. The kinetic models correlate the adsorbed amount of ions with time. Lagergren presented Eq. (6) for pseudo-first-order reactions [43]:

$$\frac{dq_t}{d_t} = k_1(q_e - q_t) \tag{6}$$

where q_e and q_t are the ion concentrations in the solid phase at equilibrium and at time t respectively, and k_1 is the model constant (min^{-1}). After integrating Eq. (6) with the boundary conditions (q_t = 0 to $q_t = q_t$ and t = 0 to $t = t$), the linear form (Eq. (7)) was obtained.

$$\frac{1}{q_t} = \frac{k_1}{q_e t} + \frac{1}{q_e} \tag{7}$$

The rate constant k_1 was determined from the plot of $1/q_t$ vs. $1/t$, (Fig. 9(a)), and the value of q_e was calculated from the intercept. The model variables along with the coefficients are presented in Table 2.

The plots in Fig. 9(a) manifest a linear fit with the correlation coefficient (R^2 of 0.991), and the values of k_1 and q_e were found as 5.64 min^{-1} and 141.04 mg g^{-1}, respectively. The calculated value of q_e confirms that the studied kinetic model did not fit the experimental results.

The second-order kinetic model, which describes the chemical adsorption, can be expressed as [44]:

$$\frac{dq_t}{d_t} = k_2(q_e - q_t)^2 \tag{8}$$

where k_2 is the model constant (g (mg min)$^{-1}$). After integrating Eq. (8) with the boundary conditions (q_t = 0 to $q_t = q_t$ at t = 0 to $t = t$), Eq. (9) was achieved.

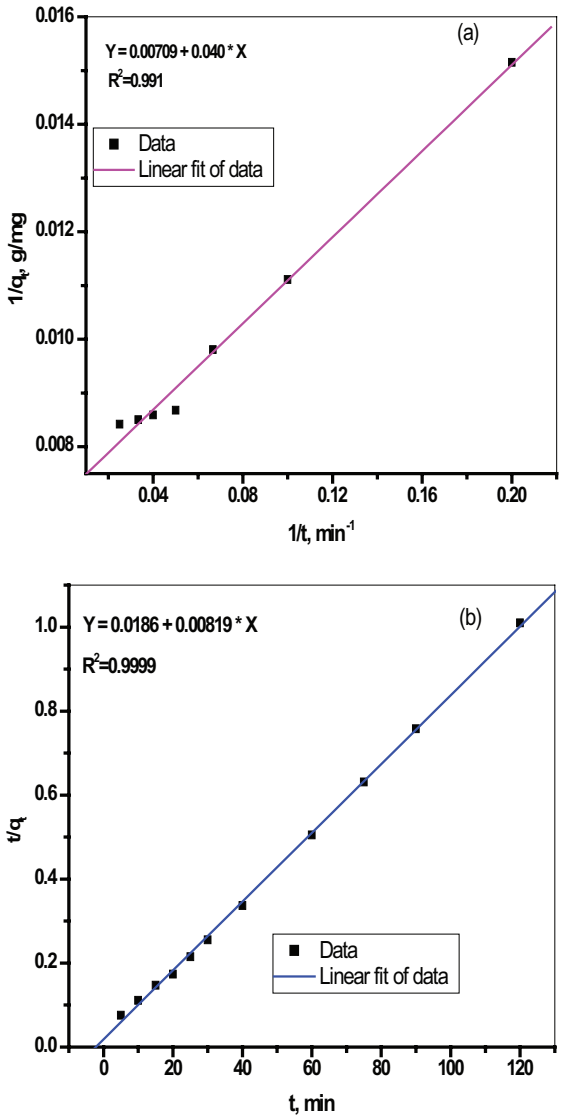

Fig. 9. Pseudo first-order kinetic model plot (a) and pseudo second order kinetic model plot (b) for adsorption of Hg (II).

$$\frac{t}{q_t} = \frac{1}{k_2 q_e^2} + \frac{t}{q_e} \tag{9}$$

The model variables were calculated from the plot of t/q_t vs. t (Fig. 9(b)). The plot shows a linear relation, while the model parameters with the correlation coefficient R^2 are presented in Table 3.

The results in Table 3 confirm that the adsorption of Hg (II) on GAD-PTSC fits the pseudo-second-order kinetic model [45].

The values of correlation coefficient R^2 and adsorption capacity q_e for the second-order kinetics model were 0.9999 and 122.1 respectively. Which indicates the favored chemical adsorption process. As the value of R^2 is near to unity, the current result agrees with the previous study on the adsorption of Hg (II) on thiosemicarbazide functional materials [42]. It could be inferred that a five-membered ring could be formed

Table 3
The variables of kinetic models for adsorption of Hg (II) onto GAD-PTSC

Kinetic model	Parameters	R^2
Pseudo first order	k_1 = 5.64	0.991
	q_e =141.04	
Pseudo second order	$K_2 = 3.60 \times 10^{-3}$	0.9999
	q_e = 122.100	

through the complexation between Hg (II) and GAD-PTSC, hence, supporting the formation of chelates [46].

3.2.4. Isothermal studies

3.2.4.1. Effect initial metal ion concentration The adsorption of Hg (II) on GAD-PTSC was studied at different metal ion concentrations (within the range 10–200 mg L^{-1}). The adsorbed amount of Hg (II) against the initial Hg(II) ion concentration is presented in Fig. 10. The obtained results revealed that the adsorbed amount of Hg (II) on GAD-PTSC firstly increased with the increasing ion concentrations then reached a steady value. This finding could be due to the saturation of the resin active sites with increasing the concentration of ions competing on the active groups. The adsorption isotherm studies were performed to investigate the adsorption mechanism. The Langmuir and Freundlich isotherm models were applied to the obtained experimental results. The Langmuir isotherm model can be expressed as:

$$\frac{C_e}{q_e} = \frac{1}{K_L} + \frac{C_e}{q_{\max}} \tag{10}$$

where q_e and C_e are the equilibrium adsorption capacity (mg g^{-1}) and the equilibrium metal ion concentration (mg L^{-1}) in solution, respectively, q_m is the maximum adsorbed amount of Hg (II) on GAD-PTSC (mg g^{-1}), and K_L is the Langmuir constant (L mg^{-1}). The Langmuir isotherm model describes a monolayer adsorption at homogeneous sites on the adsorbent surface. The Langmuir isotherm plot is illustrated in Fig. 11(a), and the model parameters are presented in Table 4. The Langmuir isotherm model assumes that all adsorption sites are energetically identical and the binding force decreases with increasing the distances of the adsorbates from the adsorbent surface.

The Freundlich isotherm model assumes that adsorption occurs at multilayer on heterogeneous surfaces and energetically at different sites, and it can be expressed using Eq. (11).

$$\ln q_e = \ln k_f + \frac{1}{n}\ln C_e \tag{11}$$

where K_f and n are the sorption capacity and the sorption intensity constants, respectively. The Freundlich plot is illustrated in Fig. 11(b), and the calculated model parameters are presented in Table 4.

It is evident from Table 4 that the Langmuir isotherm model fitted well (R^2 > 0.999) with the

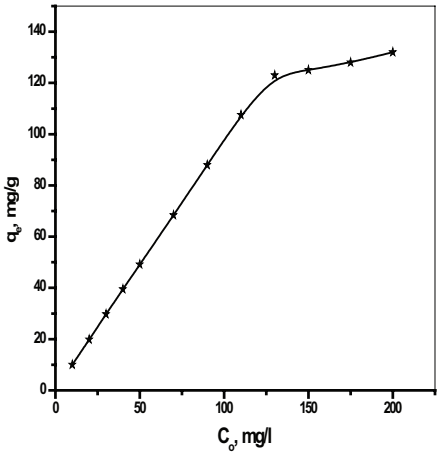

Fig. 10. Effect of initial Hg(II) concentration on the adsorbed amount onto GAD-PTSC; adsorbent dose 0.1 g/100 mL, temperature 25°C, and pH 6.

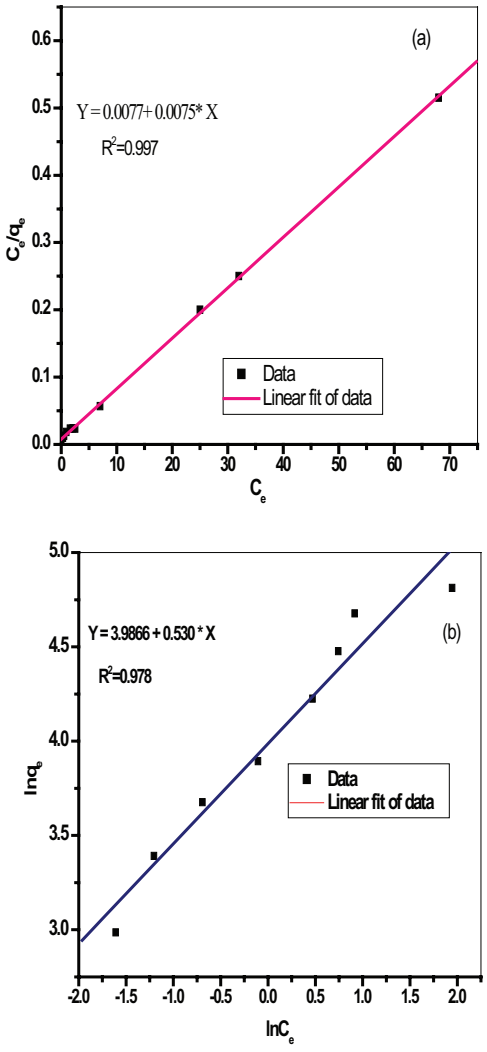

Fig. 11. Langmuir plot (a) and Freundlich plot (b) for the adsorption of Hg (II) on GAD-PTSC.

experimental results as compared with the Freundlich isotherm (R^2 > 0.978), suggesting a monolayer adsorption. The maximum adsorption of Hg (II) on GAD-PTSC was found from Langmuir model as 133.33 mg g^{-1}, reflecting a high affinity of GAD-PTSC toward Hg^{2+}.

The separation factor constant (R_L) was calculated to determine the suitability of the process for the removal of Hg (II) from aqueous solutions. If R_L > 1.0, the process is unfavorable; if R_L = 1, the process is linear (0 < R_L < 1) and favorable; and if R_L = 0, the process is irreversible [46]. The values of R_L were calculated using Eq. (12).

$$R_L = \frac{1}{1 + C_0 K_L} \tag{12}$$

where K_L is the Langmuir equilibrium constant and *Co* is the initial Hg (II) concentration (10–200 mg L^{-1}). The values of R_L were found in the range of 0 and 1, confirming a favorable and suitable process for the removal of Hg (II) from aqueous solutions. Based on the aforesaid results, the GAD-PTSC-Hg (II) chelating mechanism is depicted in Fig. 12.

3.2.5. Recycling of depleted resin

The regenerated resin was studied in repeated adsorption cycles. The regenerated resin showed efficiency of 92% and 91% after the first and second adsorption cycles respectively. This finding helps in reducing the decontamination process cost as the usage of depleted resin could save the materials synthesis cost.

3.2.6. Comparing the adsorption capacity with different studies

In Table 5 the maximum adsorption capacity of Hg (II) using different adsorbent materials are presented compared with GAD-PTSC. It could be revealed that the adsorption capacity of Hg (II) onto GAD-PTSC is potentially encouraging.

Table 4
Isotherm model parameters for adsorption of Hg (II) onto GAD-PTSC

Kinetic model	Parameters	R^2
Langmuir	K_L = 129.87 q_{max} =133.33	0.9996
Freundlich	K_f = 53.69 n = 1.886	0.978

Table 5
Comparison of maximum adsorption capacity of various adsorbents for Hg (II) ions

Adsorbent	Maximum adsorption capacity (mg g^{-1})	References
Magnetic zirconium phosphate	181.8	[47]
Polyaniline-Zr(IV) phosphoborate	153.8	[48]
Starch/SnO_2 nanocomposite	192	[49]
Gum Arabic dialdehyde phenylthiosemicarbazone	133.3	This work
Ti(IV) iodovanadate cation exchanger	21.38	[50]
Buckwheat hulls	82.1	[51]
Alizarin red-S-modified amberlite IRA-400 resin	303.03	[52]
Nickel ferrite bearing nitrogen-doped mesoporous carbon	476.2	[53]

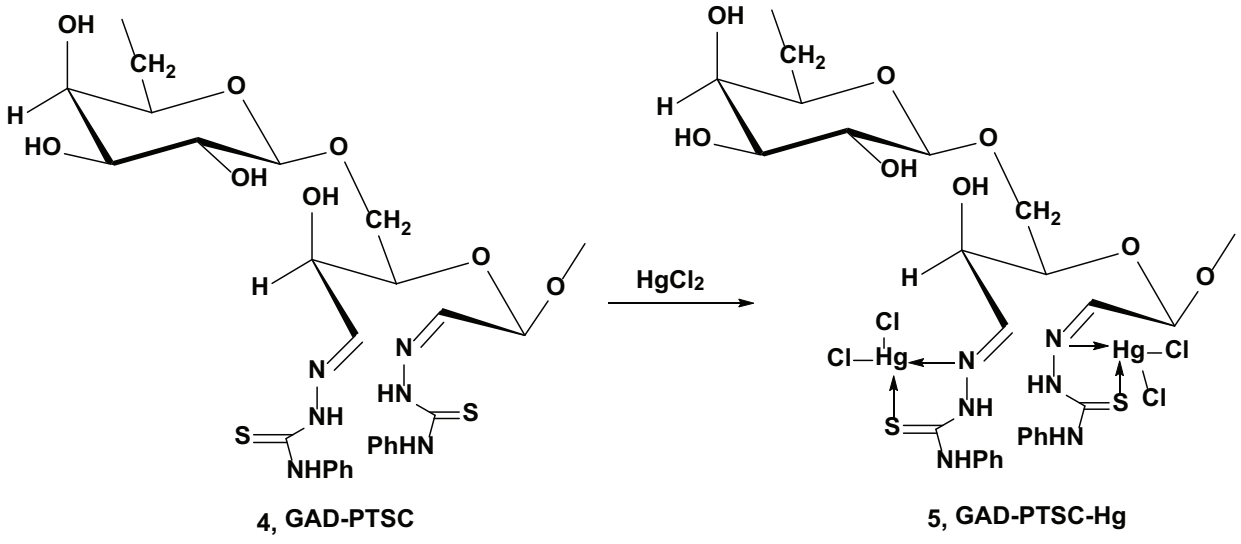

Fig. 12. Gum acacia dialdehyde-2,3-bis (4-phenylthiosemicarbazone)-mercuric complex.

4. Conclusion

In this research, a novel chelating adsorbent GAD-PTSC was synthesized for the removal of Hg (II) from aqueous solutions. The maximum adsorption of Hg (II) at 25°C was found as 125 mg g^{-1} at pH 5.5. The adsorption of Hg (II) ions on GAD-PTSC followed a pseudo-second-order kinetic model with $k_2 = 3.60 \times 10^{-3}$, $q_e = 133.10$ with a correlation coefficient of 0.999. The Langmuir adsorption isotherm model also showed good fitting with the experimental results with maximum adsorption capacity of 133.33 mg g^{-1} and correlation coefficient of 0.999, confirming the presence of chemical interaction between Hg (II) and GAD-PTSC.

Acknowledgment

The authors extend their appreciation to the Deanship of Scientific Research at King Khalid University for funding this work through research groups program under grant number R.G.P. 1/19/40.

References

[1] A.A. Atia, A.M. Donia, H.H. El-Nomany, Adsorption of mercury(II) on amidoxime chelating, J. Dispers. Sci. Technol., 30 (2009) 451–458.
[2] C. Jeon, K.H. Park, Adsorption and desorption characteristics of mercury(II) ions using aminated chitosan bead, Water Res., 39 (2005) 3938–3944.
[3] S. Muthusaravanan, N. Sivarajasekar, J.S. Vivek, T. Paramasivan, Mu. Naushad, J. Prakashmaran,V. Gayathri, O.K. AlDuaij, Phytoremediation of heavy metals: mechanisms, methods and enhancements, Environ. Chem. Lett., 16 (2018) 1339–1355.
[4] N. Sivarajasekar, N. Mohanraj, S. Sivamani, I. Ganesh Moorthy, Response surface methodology approach for optimization of lead(II) adsorptive removal by Spirogyra sp. biomass, Environ. Biotechnol. Res., 6 (2017) 88–95.
[5] N. Sivarajasekar, Hevea brasiliensis – a biosorbent for the adsorption of Cu(II) from aqueous solutions, Carbon Lett., 8 (2007) 199–206.
[6] W.S. Wan Ngah, C.S. Endud, R. Mayanar, Removal of copper(II) ions from aqueous solution onto chitosan and cross-linked chitosan bead, React. Funt. Polym., 50 (2002) 181–190.
[7] G.R. Kiani, H. Sheikhloie, N. Arsalani, Heavy metal ion removal from aqueous solutions by functionalized polyacrylonitrile, Desalination, 269 (2011) 266–270.
[8] B.A. Fil, R. Boncukcuoglu, A.E. Yilmaz, S. Bayar, Adsorption of Ni(II) on ion exchange resin: kinetics, equilibrium and thermodynamic studies, Korean J. Chem. Eng., 29 (2012) 1232–1238.
[9] B.A. Fil, R. Boncukcuoglu, A.E. Yılmaz, S. Bayar, Adsorption kinetics and isotherms for the removal of zinc ions from aqueous solutions by an ion-exchange resin, J. Chem. Soc. Pak., 34 (2012) 841–848.
[10] F. Liu, L. Li, P. Ling, X. Jing, C. Li, A. Li, X. You, Interaction mechanism of aqueous heavy metals onto a newly synthesized IDA-chelating resin: isotherms, thermodynamics and kinetics, Chem. Eng. J., 173 (2011) 106–114.
[11] L. Li, F. Liu, X. Jing, P. Ling, A. Li, Displacement mechanism of binary competitive adsorption for aqueous divalent metal ions onto a novel IDA-chelating resin: isotherm and kinetic modeling, Water Res., 45 (2011) 1177–1188.
[12] F. An, B. Gao, X. Dai, Efficient removal of heavy metal ions from aqueous solution using salicylic acid type chelate adsorbent, J. Hazard. Mater., 192 (2011) 956–962.
[13] F. Ge, M.M. Li, H. Ye, B.X. Zhao, Effective removal of heavy metal ions Cd(II), Zn(II), Pb(II), Cu(II) from aqueous solution by polymer-modified magnetic nanoparticles, J. Hazard. Mater., 211–212 (2012) 366–372.
[14] M. Monier, D.A. Abdel-Latif, Preparation of cross-linked magnetic chitosan-phenylthiourea resin for adsorption of Hg(II), Cd(II) and Zn(II) ions from aqueous solutions, J. Hazard. Mater., 209–210 (2012) 240–249.
[15] H. Sepehrian, S.J. Ahmadi, S.Waqif-Husain, H. Faghihian, H. Alighanbari, Adsorption studies of heavy metal ions on mesoporous aluminosilicate, novel cation exchanger, J. Hazard. Mater., 176 (2010) 252–256.
[16] F. Ma, R. Qu, C. Sun, C.Wang, C. Ji, Y. Zhang, P. Yin, Adsorption behaviors of Hg(II) on chitosan functionalized by amino-terminated hyperbranched polyamidoamine polymers, J. Hazard. Mater., 172 (2009) 792–801.
[17] P. Girods, A. Dufour, V. Fierro, Y. Rogaume, C. Rogaume, A. Zoulalian, A. Celzard, Activated carbons prepared from wood particleboard wastes: characterization and phenol adsorption capacities, J. Hazard. Mater., 166 (2009) 491–501.
[18] K. Sui, Y. Li, R. Liu, Y. Zhang, X. Zhao, H. Liang, Y. Xia, Biocomposite fiber of calciumalginate/multi-walled carbon nanotubes with enhanced adsorption properties for ionic dyes, Carbohydr. Polym., 90 (2012) 399–406.
[19] A. Ofomaja, Y. Ho, Equilibrium sorption of anionic dye from aqueous solution by palm kernel fibre as sorbent, Dyes Pigm., 74 (2007) 60–66.
[20] F. Zhang, Z. Zhao, R. Tan, Y. Guo, L. Cao, L. Chen, J. Li, W. Xu, Y. Yang, W. Song, Selective and effective adsorption of methyl blue by barium phosphate nanoflake, J. Colloid Interface Sci., 386 (2012) 277–284.
[21] A.X. Yan, S. Yao, Y.G. Li, Z.M. Zhang, Y. Lu, W.L. Chen, E.B. Wang, Incorporating polyoxometalates into a porous MOF greatly improves its selective adsorption of cationic dyes, Chem. Eur. J., 20 (2014) 6927–693.
[22] M.J Zohuriaan-Mehr, A. Pourjavadi, M. Salehi-Rad, Modefied CMC.2. Novel Carboxymethylcellulose-base Poly(amidoxime) chelating resin with high sorption capacity, React. Funct. Polym., 61(2004) 23–31.
[23] G.S.Chanuhan, S.C. Jaswal, M. Verma, Post functionalization of carboxymethylated starch and acrylonitrile based networks through amidoximation for use as ion sorbents, Carbohydr. Polym., 66 (2006) 435–443.
[24] F.M.B. Coutinho, S.M. Rezende, C.C.R. Barbosa, Influence of the morphological structure of macroreticular amidoxime resins on their complexation capacity, React. Funct. Polym., 49 (2001) 235–248.
[25] A. Spanova, D. Horak, E. Soudkova, B. Rittich, Magnetic hydrophilic methacrylate-based polymer microspheres designed for polymerase chain reactions applications, J. Chromatography B, 800 (2004) 27–32.
[26] M. Yamaura, R.L. Camilo, M.C.F.C. Felinto, Synthesis and performance of organic-coated magnetite particles, Alloys Comp., 244 (2002) 152–156.
[27] A.A. Atia, A.M. Donia, A.E. Shahin, Studies on the uptake behavior of a magnetic Co3O4-containing resin for Ni(II), Cu(II) and Hg(II) from their aqueous solutions, Sep. Purif. Technol., 46 (2005) 208–213.
[28] A.A. Atia, Studies on the interaction of mercury(II) and uranyl(II) with modified chitosan resins, Hydrometallurgy, 80 (2005) 13–22.
[29] A.A. Atia, A.M. Donia, S.A. El-Enein, A.M. Yousif, Effect of chain length of aliphatic amines immobilized on a magnetic glycidyl methacrylate resin towards the uptake behavior of Hg(II) from aqueous solutions, Sep. Sci. Technol., 42 (2007) 403–420.
[30] L. Domingue, Z. Yue, J. Economy, C.L. Mangun, Design of polyvinyl alcohol mercaptyl fibers for arsenite chelation, React. Funct. Polym., 53 (2002) 205–215.
[31] J.M. Robert, D.L. Rabenstein, Indirect detection of mercury-199 nuclear magnetic resonance spectra of methylmercury complexes, Anal. Chem., 63 (1991) 2674–2679.
[32] O.H. M. Idris, PA Williams, GO Philips, Characterization of gum from Acacia Senegal trees of different age and location using multi detection gel permeation chromatography, Food Hydrocolloids, 12 (1998) 379–388.
[33] K.K. Taha, R.H. Elmahi, E.A. Hassan, S.E. Ahmed, M.H. Shyoub, Analytical study on three types of gum from Sudan, J. For. Prod. Ind., 1 (2012) 11–16.

[34] S.B. Novakovic, G.A. Bogdanovic, V.M. Leovac, Transition Metal Complexes with Thiosemicarbazide-Based Ligands. Part L. Synthesis, Physicochemical Properties and Crystal Structures of Co(II) Complexes with Acetone S-Methyliso-Thiosemicarbazone, Polyhedron, 25 (2006) 1096–1104.
[35] K. Peariso, C.W. Goulding, S. Huang, R.G. Matthews, J.E. Penner-Hahn, Characterization of the zinc binding site in methionine synthase enzymes of Escherichia coli: the role of zinc in the methylation of homocysteine, J. Am. Chem. Soc., 120 (1998) 8410–8416.
[36] G. Sharma, A. Kumar, K. Devi, S. Sharma, Mu. Naushad, A.A. Ghfar, T. Ahamad, F.J. Stadler, Guar gum-crosslinked-Soya lecithin nanohydrogel sheets as effective adsorbent for the removal of thiophanate methyl fungicide, Int. J. Biol. Macromol., 114 (2018) 295–305.
[37] M. Farooq, S. Sagbas, M. Sahiner, M. Siddiq, M. Turk, N. Aktas, N. Sahiner, Synthesis, characterization and modification of Gum Arabic microgels for hemocompatibility and antimicrobial studies, Carbohydr. Polym., 156 (2017) 380–389.
[38] J. Stefanovic, D. Jakovljevic, G. Gojgic-Cvijovic, M. Lazic, M. Vrvic, Synthesis, characterization, and antifungal activity of nystatin-gum Arabic conjugates, J. Appl. Polym. Sci., 127 (2013) 4736–4743.
[39] A. Abdullah Alqadami, Mu. Naushad, Z. Abdullah Alothman, and A.A. Ghfar, Novel metal–organic framework (MOF) based composite material for the sequestration of U(VI) and Th(IV) metal ions from aqueous environment, ACS Appl. Mater. Interfaces, 9 (2017) 36026–36037.
[40] K.Y. Shin, J.Y. Hong, J. Jang, Heavy metal ion adsorption behavior in nitrogendoped magnetic carbon nanoparticles: isotherms and kinetic study, J. Hazard. Mater., 190 (2011) 36–44.
[41] S.L. Sun, A.Q. Wang, Adsorption properties of carboxymethyl-chitosan and crosslinked carboxymethyl-chitosan resin with Cu(II) as template ions, Sep. Purif. Technol., 49 (2006) 197–204.
[42] G. Pelosi, Thiosemicarbazone metal complexes: from structure to activity, Open Crystallogr. J., 3 (2010) 16–28.
[43] S. Lagergren, About the theory of so-called adsorption of soluble substances, K. Sven. vetensk.akad. handl., 24 (1898) 1–39.
[44] Y.S. Ho, E. McKay, The kinetics of sorption of basic dyes from aqueous solution by sphagnum moss pea, Can. J. Chem. Eng., 76 (1998) 822–827.
[45] Y.S. Ho, G. McKay, Pseudo-second order model for sorption processes, Process Biochem., 34 (1999) 451–465.
[46] L. Zhou, C. Shang, Z. Liu, G. Huang, A.A. Adesina, Selective adsorption of uranium(VI) from aqueous solutions using the ion-imprinted magnetic chitosan resins, J. Colloid Interface Sci., 366 (2012) 165–172.
[47] T. Ahamad, Mu. Naushad, B.M. Al-Maswari, J. Ahmed, Z.A. ALOthman, S.M. Alshehri, A.A. Alqadami, Synthesis of a recyclable mesoporous nanocomposite for efficient removal of toxic Hg2+ from aqueous medium, J. Ind. Eng. Chem., 53 (2017) 268–275.
[48] R. Bushra, Mu. Naushad, G. Sharma, A. Azam, Z.A. Alothman, Synthesis of polyaniline based composite material and its analytical applications for the removal of highly toxic Hg2+ metal ion: antibacterial activity against E. coli, Korean J. Chem. Eng., 34 (2017) 1970–1979.
[49] Mu. Naushad, T. Ahamad, G. Sharma, A.H. Al-Muhtaseb, A.B. Albadarin, M.M. Alam, Z.A. ALOthman, S.M. Alshehri, A.A. Ghfar, Synthesis and characterization of a new starch/SnO2 nanocomposite for efficient adsorption of toxic Hg2+ metal ion, Chem. Eng. J., 300 (2016) 306–316.
[50] Mu. Naushad, Z.A. ALOthman, Md. Rabiul Awual, M.M. Alam, G.E. Eldesoky, Adsorption kinetics, isotherms, and thermodynamic studies for the adsorption of Pb2+ and Hg2+ metal ions from aqueous medium using Ti(IV) iodovanadate cation exchanger, Ionics, 21 (2015) 2237–2245.
[51] Z. Wang, P. Yin, R. Qu, H. Chen, C. Wang, S. Ren, Adsorption kinetics, thermodynamics and isotherm of Hg(II) from aqueous solutions using buckwheat hulls from Jiaodong of China, Food Chem., 136 (2013) 1508–1514.
[52] Mu. Naushad, S. Vasudevan, G. Sharma, A. Kumar, Adsorption kinetics, isotherms, and thermodynamic studies for Hg2+ adsorption from aqueous medium using alizarin red-S-loaded amberlite IRA-400 resin, Desal. Wat. Treat., 57 (2016) 18551–18559.
[53] Mu. Naushad, T. Ahamad, B.M. Al-Maswari, A.A. Alqadami, S.M. Alshehri, Nickel ferrite bearing nitrogen-doped mesoporous carbon as efficient adsorbent for the removal of highly toxic metal ion from aqueous medium, Chem. Eng. J., 330 (2017) 1351–1360.